LARGE EDDY SIMULATION OF A TURBULENT NON-PREMIXED FLAME

Marco Kupiainen
Department of Numerical Analysis and Computer Science,
Royal Institute of Technology
S-144 00, Stockholm, Sweden
marcok@nada.kth.se

Christer Fureby
Department of Weapons and Protection, Warheads and Propulsion
The Swedish Defence Research Agency, FOI
S-172 90, Stockholm, Sweden
fureby@foi.se

ABSTRACT

Improved mixing of a jet with its surroundings is of interest in many applications that demand enhanced combustion of injected fuel and background oxidizer (in e.g. SI engines, ram- and scramjet engines and jet flame afterburning). In this context, there is a great interest in understanding and predicting the local nature of jet instabilities and their non-linear development in space and time. The vorticity dynamics and the mixing, determine the heat release pattern within the flame, and by understanding these processes it is possible to select optimal conditions to improve jet combustion. Here, we investigate non-reactive and reactive round jets using Large Eddy Simulation (LES). The LES equations are closed using the one equation eddy viscosity and the localized dynamic kinetic energy subgrid models, whereas the combustion is modeled by a truncated Arrhenius chemistry model. Grid refinements have been performed to study the influence of different grids on the solution. For the non-reacting jet good agreement with experimental data is found, whereas for the reacting jet the flow field is reasonably well predicted, but less good agreement is found for the thermodynamic quantities.

INTRODUCTION

Turbulent non-premixed jets are impotant in many engineering applications including flows in diesel engines and aircraft turbines. In such systems combustion occurs only if fuel and oxidizer are properly mixed at the molecular level. After entrainment of fuel and oxidizer in the unsteady coherent structures, micromixing, acting at smaller scales, brings fuel and oxidizer in contact with each other on the microscopic level within the reaction zone where products are formed and exothermicity occurs. Although turbulent mixing is responsible for stirring the reactants at large scales, it contributes to the molecular mixing only indirectly by increasing the scalar variance and hence the scalar gradients. Molecular mixing, on the other hand, essentially occurs at the smallest scales by expulsion of the scalar variance. The rate of molecular mixing is therefore represented by the scalar dissipation rate - being the most important parameter in the description of non-premixed combustion, providing a measure of the peak reaction rate.

Numerical prediction methods for non-premixed flames can be divided into Direct Numerical Simulations (DNS) in which all time and space scales are resolved, e.g. (Vervish and Poinsot, 1998), Large Eddy Simulations (LES), e.g. (Fureby, 2001) and (Menon, 2001), in which only the larger scales are resolved and subgrid models are used to represent the effects of the small scales upon the large resolved scales, and Reynolds Averaged Navier Stokes (RANS) models, e.g. (Jones, 1993), in which all scales are modeled. DNS, LES and RANS can be considered as complementary methods, providing different levels of information and accuracy, and finding different areas of application. The description of chemical kinetics and molecular diffusion is complicated and moreover, kinetics and species diffusion influence each other and occur mainly on subgrid scales together with effects due to counter-gradient diffusion, flame generated turbulence, and flame instability.

In this paper we consider LES of a turbulent non-premixed $CO/H_2/N_2$-air jet flame. Experimental test data are provided by Sandia, (Sandia, 2003), for validation of the numerical simulation. The aim is to compare predictions from LES calculations with experimental data such as the mean velocity, temperature and species concentrations on the centerline of the flame and at cross-sections downstream of the nozzle. Furthermore, we wish to examine the intrinsic physics of both non-reacting and reacting jets with emphasis on the differences between reacting and non-reacting jets.

LES COMBUSTION MODELS

The equations of reactive flow are the conservation and balance equations of mass, momentum and energy, (Lions, 1996), supplemented by constitutive equations, describing advection, diffusion and chemical reaction, e.g. (Oran and Boris, 1987). Numerical simulation of turbulent reacting flows includes dealing with a wide range of length and time scales. The largest scales are related to the geometry whilst the smallest are associated with dissipation of turbulence by viscosity. Chemical reactions have their own spectrum of scales, and different interactions between the chemistry and the turbulence are possible depending on the overlap of the scales. To handle this spectrum of scales, the equations of reactive flow are low-pass filtered in LES to remove the scales below the filter width Δ (typically chosen to be the grid size). Hence,

$$\partial_t(\overline{\rho}) + \nabla \cdot (\overline{\rho}\widetilde{\mathbf{v}}) = 0, \quad (1)$$

$$\partial_t(\overline{\rho}\widetilde{\mathbf{v}}) + \nabla \cdot (\overline{\rho}\widetilde{\mathbf{v}} \otimes \widetilde{\mathbf{v}}) = -\nabla\overline{p} + \nabla \cdot (\overline{\mathbf{S}} - \mathbf{B}), \quad (2)$$

$$\partial_t(\overline{\rho}\widetilde{Y}_i) + \nabla\cdot(\overline{\rho}\widetilde{\mathbf{v}}\widetilde{Y}_i) = \nabla\cdot\left(\overline{\mathbf{j}_i} - \mathbf{b}_i\right) + M_i\nu_{ij}\overline{\dot{\omega}_j}, \quad (3)$$

$$\partial_t(\overline{\rho}\widetilde{h} - \overline{p}) + \nabla\cdot((\overline{\rho}\widetilde{h} + \overline{p})\widetilde{\mathbf{v}}) = \overline{\mathbf{S}}\cdot\widetilde{\mathbf{D}} + \overline{\rho}\varepsilon + \nabla\cdot(\overline{\mathbf{h}} - \mathbf{b}_h), \quad (4)$$

where ρ is the density, $\mathbf{v}$ the velocity, Y_i the species mass fraction, $\mathbf{j}_i$ the species mass difffusion vector, M_i the species molar mass, ν_{ij} the stoichiometric coefficient, $\dot{\omega}_j$ the reaction rate, p the pressure, $\mathbf{S}$ the viscous stress tensor, h the enthalpy of the mixture, $\mathbf{S}\cdot\mathbf{D}$ the viscous work, $\mathbf{D} = \frac{1}{2}\left(\nabla(\mathbf{v}) + \nabla(\mathbf{v})^T\right)$ the rate of strain tensor, ε the subgrid-scale dissipation, and $\mathbf{h}$ the heat flux vector. Here, overbars $(\overline{\cdot})$ and tildes $(\widetilde{\cdot})$ denote filtering and density (or Favré) weighted filtering, respectively. Here, $\mathbf{B}$, $\mathbf{b}_i$, $\mathbf{j}_i$ and $\mathbf{b}_h$ are the subgrid species, momentum and energy transport terms which are to be modeled.

When attempting to simulate turbulent combustion we have to simplify both the flow modeling and the combustion chemistry. In the following paragraphs we outline the methods used in the present study.

Subgrid turbulence modeling

In the low-pass filtered state and constitutive equations of the subgrid, fluctuations are ignored, resulting in $\overline{p} \approx \overline{\rho}R_i(\frac{\widetilde{Y}_i}{M_i})\widetilde{T}$, $\widetilde{h} \approx \sum_i \widetilde{Y}_i(h^o_{f_i} + C_{p_i}(\widetilde{T} - T_0))$, and $\overline{\mathbf{j}_i} \approx \mathcal{D}_i\nabla\widetilde{Y}_i$, where $\mathcal{D}_i$ is the diffusivity of species i, $\overline{\mathbf{S}} \approx (\lambda + \frac{2}{3}\mu)\mathrm{tr}\widetilde{\mathbf{D}}\mathbf{I} + 2\mu\widetilde{\mathbf{D}}_D$, $\overline{\mathbf{h}} \approx \kappa\nabla\widetilde{T}$, $\mathbf{b}_i = -\mathcal{D}_k\nabla\widetilde{Y}_i$, $\mathbf{B} = \frac{2}{3}\overline{\rho}k\mathbf{I} - 2\mu_k\widetilde{\mathbf{D}}_D$ and $\mathbf{b}_h = -\kappa_k\nabla\widetilde{h}$ in which the subgrid viscosity μ_k and the subgrid diffusivities $\mathcal{D}_k$ and κ_k are parametrized using the subgrid kinetic energy k as $\mu_k = c_k\Delta\sqrt{k}$, $\kappa_k = \frac{\mu_k}{Pr_t}$ and $\mathcal{D}_k = \frac{\mu_k}{Sc_t}$, respectively. Here, $k = \frac{1}{2}\mathrm{tr}\mathbf{B}$ is obtained from the modeled transport equation,

$$\partial_t(\overline{\rho}k) + \nabla\cdot(\overline{\rho}k\widetilde{\mathbf{v}}) = -\mathbf{B}\cdot\widetilde{\mathbf{D}} + \nabla\cdot((\mu + \mu_k)\nabla k) - \overline{\rho}\varepsilon, \quad (5)$$

in which $\varepsilon = \frac{c_\varepsilon}{\Delta}k^{\frac{3}{2}}$ is the subgrid dissipation. Here, the coeffiecients c_k and c_ε are evaluated either from a $|\mathbf{k}|^{-\frac{5}{3}}$ inertial sub-range behaviour (resulting in $c_k = 0.07$ and $c_\varepsilon = 1.05$) or a dynamic procedure, using the experimentally observed scale similarity between $\mathbf{B}$ and $\mathbf{L} = \overline{\rho}(\widetilde{\widetilde{\mathbf{v}}\otimes\widetilde{\mathbf{v}}} - \widetilde{\widetilde{\mathbf{v}}}\otimes\widetilde{\widetilde{\mathbf{v}}})$ as part of the solution, (Kim and Menon, 1999). These two models will hereafter be referred to as the One Equation Eddy Viscosity (OEEVM) and the Localized Dynamic Kinetic Energy (LDKM) models, respectively.

Combustion modeling

In the present study we consider two different approaches for modeling the combustion.

Conserved scalar approach. For non-premixed combustion the treatment of the chemical source term, $M_i\nu_{ij}\dot{\omega}_j$, which is the main difficulty in reactive flow calculations, may be avoided by using a conserved scalar formalism. Using this approach the chemical reaction rates are assumed to be fast compared to the rate at which the reactants are mixed. For a global reaction mechanism, and under the assumption of equal species diffusivities ($\mathcal{D} = \mathcal{D}_i$, $\forall i$), a conservation law for a conserved scalar can be derived e.g. (Poinsot and Veynante, 2001),

$$\partial_t(\overline{\rho}\widetilde{Z}) + \nabla\cdot(\overline{\rho}\widetilde{\mathbf{v}}\widetilde{Z}) = \nabla\cdot(\mathcal{D}\nabla\widetilde{Z} - \mathbf{b}_z), \quad (6)$$

where $\mathbf{b}_z = -\mathcal{D}_k\nabla\widetilde{Z}$. The chemistry is here approximated to an equilibrium, which leads to the Burke-Schumann solution, (Burke and Schumann, 1928). Here the mass fractions are functions of Z only, i.e. $Y_i = Y_i(Z)$, where $Z = \frac{Y_F - sY_O + s}{1+s}$ and $s = \frac{M_F|\nu_F|}{M_O|\nu_O|}$. In order to account for the effects of subgrid turbulence, an assumed subgrid scale Probability Density Function (PDF) must be employed, following e.g. (Dopazo and O'Brien, 1973), such that,

$$\widetilde{Y}_i = \int_0^1\int_0^\infty Y_i(Z)\mathcal{P}(Z,\chi)d\chi dZ, \quad (7)$$

where χ is the scalar dissipation rate of $\widetilde{Z}$. Depending on the choice of the PDF, and the underlying assumptions different models can be derived, e.g. (Pitch, 2000). A common assumption is that $\widetilde{Z}$ and χ are independent and the PDFs used are Beta- and Dirac-delta distributions. Despite being a very popular method due to its relatively low computational cost and simplicity, this suffers from presuming the PDF's, which may change significantly across the flame.

Arrhenius chemistry model. The other model considered is, following the successful studies of (Grinstein and Kailasanath, 1995) and (Möller et al., 2000), a simplified moment method based on a global or reduced reaction mechanism. To this end we consider the one-step irreversible reaction mechanism,

$$\nu_F Y_F + \nu_O Y_O \rightarrow \nu_P Y_P, \quad (8)$$

with its rate determined by the Arrhenius expression,

$$\dot{\omega} = \rho^2 A e^{-\frac{T_a}{T}} Y_F Y_O. \quad (9)$$

The rate coeffiecients A and T_a are generally known for elementary reaction steps but not for global or reduced mechanisms. For the foreseable future we are limited to reduced or global mechanisms. However, systematic approaches to derive reduced reaction mechanisms and associated rate expressions are available, e.g. (Maas and Pope, 1992), but may be of limited use when using only one-step mechanisms. The rate parameters of an one-step irreversible reaction mechanism, can however be related to the laminar flame speed S_u, and the laminar flame-thickness, δ_u, e.g. (van Kalmthout, 1986). In this study we have followed the more general approach of (Mitani, 1980), to calculate the effective rate coefficients A and T_a given S_u.

When low-pass filtering the species equation (3), the species reaction rate becomes,

$$\overline{\dot{\omega}_i} = M_i\nu_i\overline{\dot{\omega}} = M_i\nu_i\overline{A(\rho^2 e^{-\frac{T_a}{T}}Y_F Y_O)}, \quad (10)$$

that cannot easily be expressed as a function of the low-pass filtered quantities. By expanding (10) in a Taylor series,

$$\overline{\dot{\omega}_i} = \nu_i M_i A\overline{\rho}^2\widetilde{Y}_f\widetilde{Y}_O e^{-\frac{T_a}{\widetilde{T}}}\left(1 + \frac{\overline{Y_F''Y_O''}}{\widetilde{Y}_F\widetilde{T}} + Q_1(\frac{\overline{Y_F''T''}}{\widetilde{Y}_F\widetilde{T}} + \frac{\overline{Y_O''T''}}{\widetilde{Y}_O\widetilde{T}}) + Q_2(\frac{\overline{Y_F''T''^2}}{\widetilde{Y}_F\widetilde{T}} + \frac{\overline{Y_O''T''}}{\widetilde{Y}_O\widetilde{T}}) + \ldots\right) \quad (11)$$

as suggested in (Pope, 1990), we see that the new quantities such as $\overline{Y_F''Y_O''}$ have to be closed using e.g. algebraic expressions. Depending on the non-linearities of the system it is however unclear how many terms are required for this series to be convergent, and furthermore, how to formulate models for each of these terms. A few such approaches have been attempted in the context of RANS, but for LES this modelling may be somewhat easier since only the subgrid effects

need to be explicitly accounted for. Here, we have however adopted the approach of (Grinstein and Kailasanath, 1995) and (Möller et al., 2000) and neglected these higher order terms.

NUMERICAL METHODS

The LES equations are here discretized using an unstructured Finite Volume (FM) method, e.g. (Hirsch, 1999). The discretization is based on Gauss theorem and a multi-step time integration scheme. High-order reconstruction of convective fluxes, using a second order monotonicity preserving scheme, and central differencing of the inner derivatives together with Crank-Nicholson time-integration gives second order accuracy in both space and time, for further details we refer to (Weller et al., 1997). Stability is enforced by using compact stenciles and by enforcing conservation of kinetic energy. The scalar equations are solved sequentially, with iteration over the coupling terms and the pressure-velocity coupling is handled with a PISO procedure, (Issa, 1985). This approach results in a CFL-number restriction; a maximum CFL number of 0.5 gives adequate stability, but a CFL number of 0.2 is used since LES attempts to resolve the dynamics of the large scales.

NON-REACTIVE JET DYNAMICS

Non-reactive jet studies have been performed to validate the flow solver and the LES models and to study the jetflow itself. The computations have been performed on a circular air jet at $Re_D = 20,000$ emerging into ambient air with a coflow velocity of U_∞. Here, $Re_D = \frac{(U_j - U_\infty)D}{\nu}$, where U_j is the jet velocity, D the diameter, and ν the viscosity. The velocity profile is assumed to be top-hat shaped, and the computational domain cylindrical with a length of $60D$ and a diameter of $20D$. A baseline grid of about 800,000 cells, refined around the jet-shear layers and around the nozzle, in the axial, radial and tangential directions is used. At the inflow zero Neumann conditions are used for the pressure whereas Dirichlet condtions are used for the velocity and all other scalars. At the outflow wave-transmissive boundary condtions are used for all variables, and at the radial boundary freestream conditions are employed.

In Figure 1 we present flow visualizations of the instantaneous jet dynamics. In contrast to the plane free mixing layer where primary two-dimensional spanwise vortex rollers are continuously supported downstream by the imposed shear, the jet velocity decreases towards the end of the potential core thus attenuating the shear supporting vortex rings in the jet. Sufficiently far downstream, three-dimensionality is the most inherent feature of jets with moderate-to-high Re_D. The streamwise vorticity has the crucial role entraining fluid from the surroundings, and large-scale vortices other than vortex rings dominate the jet dynamics further downstream. The natural instability of the initial laminar shear layer formed at the nozzle produces a virtually periodic array of vortex rings. As these vortex rings move downstream, they interact and generally coalesce with neighboring rings so that the scale and separation of the rings increase with distance from the nozzle. The rings deform and break up as a result of the vortex-vortex interactions eventually producing worm vortices and virtually isotropic turbulence. The details of the interaction mechanism are fairly well understood in non-reacting jets, but not in reacting jets.

Figures 2a and 2b show axial and radial profiles of the

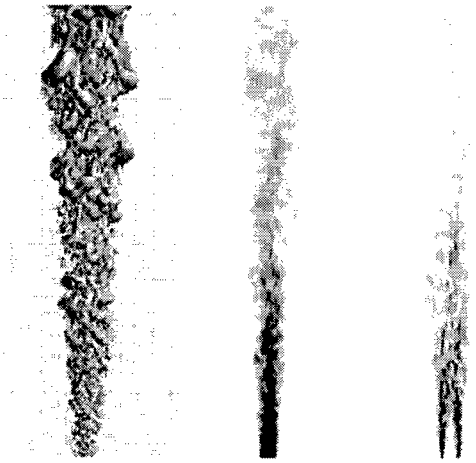

Figure 1: Perspective views from the side of the non-reactive jets shoving iso-surfaces of $Q = -\frac{1}{2}(||\widetilde{\mathbf{D}}||^2 - ||\widetilde{\mathbf{W}}||^2)$ (where $\widetilde{\mathbf{D}}$ and $\widetilde{\mathbf{W}}$ are the symmetric and skew-symmetric parts of the velocity gradient respectively) (left), contours of the axial velocity (middle) and contours of the azimuthal vorticity $\widetilde{\omega_\phi} = (\nabla \times \widetilde{\mathbf{v}})_\phi$, (right).

time-averaged axial velocity component, $\langle \mathbf{v}_x \rangle$, respectively. Comparison is made with several experimental data sets, (Cohen and Wygnanski, 1987), (Crow and Champagne, 1971) and (Lau et al., 1079), at different Re_D-numbers, since the theory suggests that due to self-similarity the profiles will collapse. Concerning the axial profile of $\langle \mathbf{v}_x \rangle$ we notice that the LES calculations result in a somewhat shorter potential core than most experimental data sets show, i.e. $3.7D$ versus about $4.2D$. This is currently believed to be caused by the lack of proper supergrid modeling, (Fureby and Grinstein, 2002). Downstream of the potential core the slope of $\langle \mathbf{v}_x \rangle$ is virtually constant, satisfying,

$$(\mathbf{v}_x - U_\infty)/U_j = \alpha D/(x - x_0), \tag{12}$$

with x_0 defining the virtual origin. From our results we find that $\alpha \approx 5.6 \pm 0.2$ and $x_0/D \approx 3.3 \pm 0.1$, which is to be compared with the theoretical values of $\alpha \approx 5.8$ and $x_0/D \approx 4$. In Figure 2b we show radial profiles of $\langle \mathbf{v}_x \rangle$ at $x/D = 5$, 10, 20, 30 and 40. Experimental data is not available within the potential core, but the agreement with data at $x/D = 40$ is good. The spreading rate $S = dr_{1/2}/dx$ satisfies $r_{1/2} = S(x - x_0)$, where $r_{1/2}$ is the half-width. From the LES we find that $S \approx 0.10 \pm 0.01$, and from experiments, S is known to vary between 0.094 and 0.105.

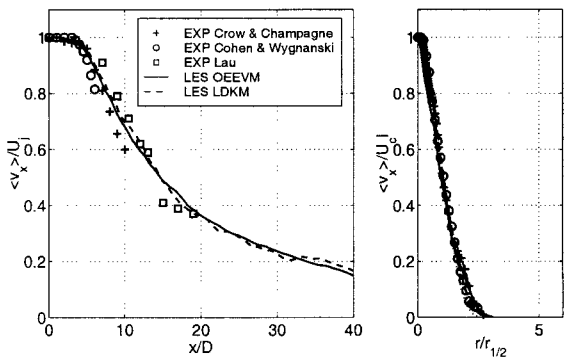

Figure 2: Axial (left) and radial (right) profiles of the time-averaged axial velocity component.

Spectral analysis is carried out to make quantitative

statements on the trends of the population of the structures in the downstream portion of the jets. The analysis is performed based on instantaneous velocity data along the jet-centerline, and Figure 3 shows the energy spectra $E(|\mathbf{k}|)$ for each of the three velocity components. All spectra show a distinct inertial range - characterizing the vortical motions consistent with the $|\mathbf{k}|^{-5/3}$ (inviscid) sub-range of the Kolmogorov K41 theory. This inertial range is typically followed by faster decay of the amplitudes due to the effect of the subgrid dissipation, which is consistent with the expected behaviour suggesting that the spectra decay more rapidly than any power of $|\mathbf{k}|$, as consistent with the underlying hypothesis of LES. The largest wavenumber for which spectral amplitudes are plotted corresponds to a wavelength of about D. Peaks of the radial and azimuthal spectra are both translated towards higher wavenumbers, signifying the fact that the radial and azimuthal flow structures evolve on a comparatively smaller scale than the axial structures.

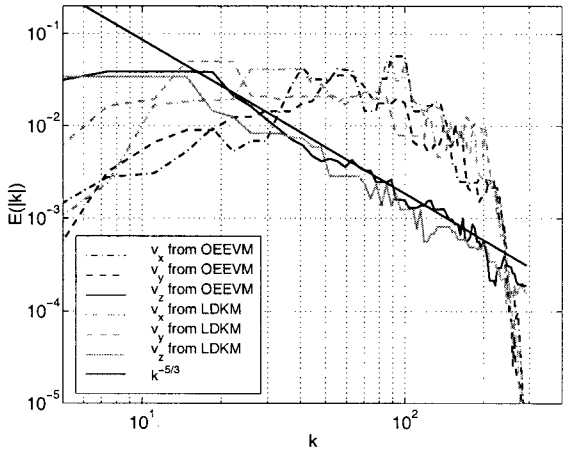

Figure 3: Velocity component based energy spectra for the non-reactive jet.

REACTIVE JET DYNAMICS

The reactive jet simulations are performed in the same computational domain, using the same spatial resolution and boundary conditions, but for the $CO/H_2/N_2$-air jet studied experimentally by (Barlow et al., 2000). The fuel composition is 40% CO, 30% H_2 and 30% N_2 by volume, the nozzle diameter is $D = 7.72\ mm$, and the jet exit velocity is $U_j = 45.0\ m/s$, resulting in a Re-number of $Re_D = 16,700$. In addition, the stoichiometric value of the mixture fraction is $Z_{st} = 0.295$. The co-flow air conditions are $U_\infty = 1.0\ m/s$ and $T_\infty = 290\ K$, respectively. Velocity measurements, using laser doppler velocimetry, were carried out at ETH in Zürich whereas the scalar and temperature measurements, using Rayleigh/Raman scattering and laser induced flourescence, were carried out at Sandia, (Sandia, 2003). The experimental data suggests that the flame is fully attached to the nozzle.

The $CO/H_2/N_2$-air system is discussed in some detail by (Drake and Blint, 1988) and from their study we may conclude that the appropriate Damköhler number ($Da = \tau_{flow}/\tau_{chemistry}$) is $Da \approx O(1)$. Here, τ_{flow} is the large-eddy turn over time ($\propto \delta_{1/2}/v_{conv}$) and $\tau_{chemistry}$ is the time scale of the CO oxidation reaction $CO + OH \rightarrow CO_2 + H$, which is the dominant heat release step. Hence, CO oxidation may be strongly coupled with the large-scale mixing, and accordingly, finite-rate chemistry models are likely to be necessary. In this study, we use the one-step global mechanism (9) with $Fu = 4CO{+}3H_2{+}3N_2$, $Ox = 3.5O_2{+}13.16N_2$ and $Pr = 4CO_2{+}3H_2O{+}16.16N_2$, with the rate-parameters (A and T_a) estimated using the method proposed in (Mitani, 1980). In the near future a more detailed, global, multi-step reaction mechanism will be investigated.

In Figure 4 we present different flow visualizations of the instantaneous reactive jet dynamics. The temperature distribution follows the distribution of the mixture fraction $\widetilde{Z}$ and as a reference the iso-surface $\widetilde{Z} = Z_{st}$ is shown in white. Burning occurs primarily at the outer edges of the jet shear layer (at $\widetilde{Z} = Z_{st}$) in the convoluted interface between reactants and products where most of the diffusive mixing takes place. The initially pulsating behaviour becomes gradually smoother as the highly vortical flow develops with downstream distance from the nozzle. The temperature distribution appears rather diffusive as an effect of the increase in heat conductivity (and molecular viscosity) due to the heat release. The cold fuel jet is clearly evident between the hot shear layers that anchor the flame, and pockets of partially burnt fuel can be observed moving downstream. Within the shear layers the primary (large-scale) entrainment and mixing takes place together with the birth of vortex rings due to the natural instability of the shear layer. The shear layers themselves develop into a sequence of large coherent structures forming three-dimensional wedges moving downstream. The jet velocity is observed to be irregular, being affected by the shear layer dynamics and the heat release taking place within the coherent structures forming the shear layer. Its radial component increases with distance from the nozzle due to a virtually linear growth of orderly wave deformation of the coherent structures. From comparison with the non-reacting case (Figure 1) it can be seen that the effects of exothermicity are mainly to delay the formation of the coherent structures and to reduce their subsequent growth. Moreover, we observe that the primary vortices in the reacting case are thicker than in the non-reacting case. This is consistent with the higher viscosity of the entrained fluid and the unfavourable density ratio between the fluids on either sides of the shear layer of the reacting jet. The formation and pairing of vortex rings leads to engulfment and entrainment of external fluid into the jet and spreading of the combustion region. The vorticity contained in the rings decreases due to diffusion, volumetric expansion and dilatation due to heat release. The rings become unstable relatively to azimuthal perturbations and break-up into longitudinal vortices.

In Figure 5 we present a comparison of the predicted and measured axial velocity component along the jet axis and at $x/D = 50$. This provides an important first level of information on the mean jet flame structure that we require the LES models to capture. As observed, good overall agreement between predictions and laboratory data is obtained for both the baseline grid and for results obtained on a coarser grid. The differences are that more details of the flow structures are resolved on the finer mesh, but their influence on the time-mean statistics is limited. The wiggles observed in the computed profiles are due to insufficiently sampled statistics, only about 50 000 time steps were used in this sampling. In comparison with the non-reactive velocity profile along the jet axis (Figure 2) we conclude that the effects of volumetric expansion increases the jet velocity between 10 and 50 jet-diameters downstream of the nozzle. The radial agreement is also reasonably good, with the experiments suggesting a somewhat wider velocity distribution far downstream.

In figure 3 the velocity component based energy spec-

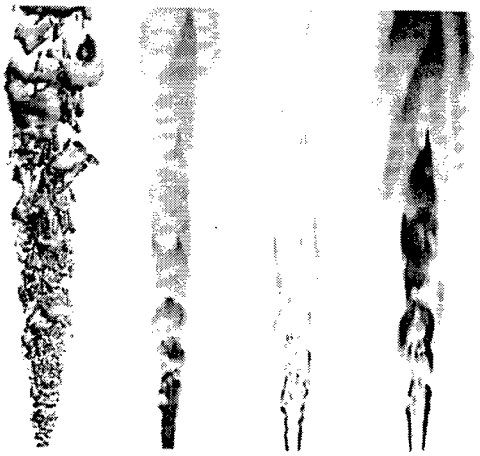

Figure 4: Perspective views from the side of the reactive jets showing (from the left): iso-surfaces of $Q = -\frac{1}{2}(||\widetilde{\mathbf{D}}||^2 - ||\widetilde{\mathbf{W}}||^2)$, contours of the axial velocity, azimuthal vorticity and temperature, respectively.

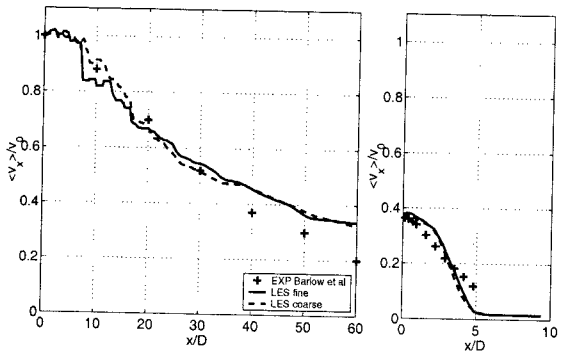

Figure 5: Time averaged axial velocity, along the centerline (left) and at the cross section $x/D = 50$ (right).

tra $E(|\mathbf{k}|)$ was presented for the non-reacting jets. Similarly we show in Figure 6 the corresponding velocity component based energy spectra $E(|\mathbf{k}|)$ for the reactive jet. As for Figure 3 the analysis is performed based on instantaneous velocity data along the jet-centerline. Considering first the energy distribution of the axial velocity of the reacting jet we see that virtually all axial modes have higher energy than in the non-reacting jet. For the radial and azimuthal components, however, less energy is contained in the axial modes for the reacting jet as compared to the non-reacting jet. For the total energy spectra the reacting jet has higher energy in virtually all modes, with a preferential amplification in the wave-number range $|\mathbf{k}| \in [10, 80]$. At higher wave-numbers a distinct but fairly short inertial sub-range, characterizing the vortical motions consistent with the $|\mathbf{k}|^{-5/3}$ (inviscid) sub-range of the Kolmogorov K41 theory, can be seen. These differences are caused mainly by the volumetric expansion caused by the chemical exothermicity, and by the baroclinic torque $(\nabla\bar{\rho} \times \nabla\bar{p})$ affecting the vorticity distribution.

In Figure 7 we present instantaneous scatter plots of temperature, $\widetilde{T}$, versus mixture fraction, $\widetilde{Z}$, at $x/D = 10$ (left) and $x/D = 50$ (right). These plots are constructed by collecting numerical data at each plane at an arbitrary instant of time. For this particular reacting $CO/H_2/N_2$-air mixture the stoichiometric value of the mixture fraction is $Z_{st} = 0.296$, which is shown as the dashed vertical lines. In the fast chemistry limit the flame sheet would be located at Z_{st}. The shift in flame location from this value and the scatter observed are due to finite-rate chemistry effects, be-

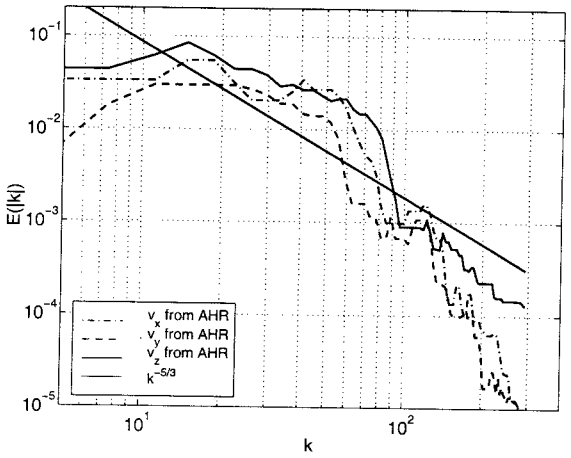

Figure 6: Velocity component based energy spectra for the reactive jet.

ing quite considerable at $x/D = 10$. In particular we find strong scatter in $\widetilde{T}$ on the fuel-rich side, suggesting high levels of intermittency and large scale mixing. Far downstream, at $x/D = 50$, we only observe points on the lean side of Z_{st} indicative of complete combustion as can be expected. The general trends are in reasonable agreement with the measurement data, e.g. Figure 16 in (Barlow et al., 2000). The main difference is that the LES calculations predicts a too rapid temperature increase along the jet centerline as compared to the experimental data. This is however not fully consistent with the good agreement found for the axial velocity component as shown in Figure 5.

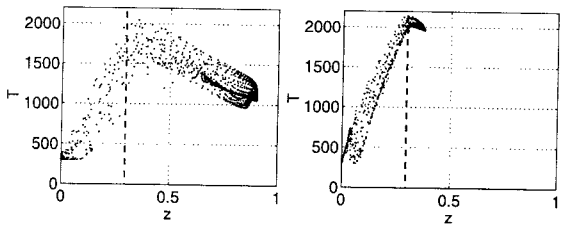

Figure 7: Instantaneous scatter plots of temperature, $\widetilde{T}$, versus mixture fraction, $\widetilde{Z}$, at $x/D = 10$ (left) and $x/D = 50$ (right).

SUMMARY AND CONCLUSIONS

Results of LES calculations of spatially developing, non-reacting, and reacting circular jets have been presented. The main focus of this work has been on (i) comparing predictions from LES calculations with measurement data, (ii) comparing results from non-reactive jet simulations with reactive jet simulations, and (iii) discussing the key features of the reactive jet. Jets with a moderate Re_D-number of about 20,000 have been investigated, and in the case of the reactive jet we considered a $CO/H_2/N_2$-air jet emanating into ambient air. The LES equations were closed by conventional and dynamic eddy-viscosity subgrid models for the subgrid stress and flux terms, whereas simplified moment methods were used to close the reaction rate terms in the species equations. To this end we used an irreversible one-step reaction mechanism with its rate parameters determined from the laminar flame speed.

For the non-reacting case very good qualitative and quantitative agreement between predictions and measure-

ment data are obtained. For the LES calculations we find virtually no differences in results obtained using the different subgrid models. Grid refinement does not affect any of the investigated first and second order statistical profiles, but provides a more detailed picture of the fluid dynamics. For the reacting case the flow field is reasonably well predicted, independent of subgrid models. Refining the grid increases the resolution of the flow variables, but does not affect the statistical moments investigated here. The simulation of combustion, however, is sensitive to which model is used. The simple one-step, irreversible one-step global reaction meachnism used in this study is too simple to describe all the couplings between the fluid dynamics and the chemistry, and will be replaced by more accurate mechanisms in the near future.

ACKNOWLEDGEMENTS

The authors greatfully acknowledge the financial support of SAAB Bofors Dynamics AB (with J. Ekeroot as contact monitor) thorugh The Parallel Scientific Computer Institute at KTH. These computations were performed with an earlier research version of the FOAM code, for further details see `http://www.nabla.co.uk`.

*

References

Barlow, R. S., Fiechtner, G. J., Carter, C., and Chen, J.-Y. (2000). Experiments on the scalar structure of turbulent CO/H2/N2 jet flames. *Combustion and Flame*, **120**:544–569.

Burke, S. P. and Schumann, T. E. W. (1928). Diffusion flames. *Industrial and Engineering Chemistry*, **20**:998–1005.

Cohen, J. and Wygnanski, I. (1987). The evolution of instabilities in the axisymmetric jet. Part 1, the linear growth of disturbances near the nozzle. *Journal of Fluid Mechanics*, **176**:191.

Crow, S. C. and Champagne, F. (1971). Orderly structure in jet turbulence. *Journal of Fluid Mechanics*, **48**:547.

Dopazo, D. and O'Brien, E. E. (1973). Statistical treatment of non-isothermal chemical reactions in turbulence. *Computational Science and Technology*, page 99.

Drake, M. C. and Blint, R. J. (1988). Structure of laminar opposed-flow diffusion flames with CO/H2/N2 fuel. *Comb. Sci. and Tech.*, **61**:187.

Fureby, C. (2001). Towards large eddy simulation of complex flows. In Friedrichs, R. and Rodi, W., editors, *Direct and Large Eddy Simulation IV*. Kluwer, The Netherlands.

Fureby, C. and Grinstein, F. F. (2002). Recent progress on MILES for high re flows. *Journal of Computational Physics*, **181**:68.

Grinstein, F. F. and Kailasanath, K. K. (1995). Three dimensional numerical simulations of unsteady reactive square jets. *Combustion and Flame*, **100**:p.2, and p. 192.

Hirsch, C. (1999). *Numerical Computation of Internal and External Flows*, volume 1 and 2. J. Wiley and Sons.

Issa, R. I. (1985). Solution of the implicitely discretized fluid flow equations by operator splitting. *Journal of Computational Physics*, **62**.

Jones, W. P. (1993). Turbulence modeling and numerical solution methods for variable density and combusting flows. In Libby, P. A. and Williams, F. A., editors, *Turbulent Reacting Flows*. Academic Press, London.

Kim, W.-W. and Menon, S. (1999). A new incompressible solver for large-eddy simulations. *Int. Journal of Numerical Fluid Mechanics*, **31**:983.

Lau, J. C., Morris, P. J., and Fisher, . J. (1079). Measurements in subsonic and supersonic free jets using a laser velocimeter. *J. Fluid MEch.*, **93**:1.

Lions, P. L. (1996). *Mathematical Topics in Fluid Mechanics*. Oxford Science Publications, Oxford.

Maas, U. and Pope, S. B. (1992). Simplifying chemical kinetics: Intrinsic low dimensional manifolds in composition space. *Combution and Flame*, **88**:239.

Menon, S. (2001). Subgrid combustion modeling for large-eddy simulations of single and two-phase flows. In Friedrichs, R. and Rodi, W., editors, *Direct and Large Eddy Simulation IV*. Kluwer, The Netherlands.

Mitani, T. (1980). Propagation velocities of two-reactant flames. *Comb. Sci. and Tech.*, **21**:175.

Möller, S. I., Lundgren, E., and Fureby, C. (2000). Large eddy simulation of unsteady combustion. In *26:th Int. Symposium on Combustion*, page 41.

Oran, E. S. and Boris, J. P. (1987). *Numerical Simulation of Reactive Flows*. Elsevier, New York.

Pitch, H. (2000). Scalar Mixing and Dissipation Rate in Large Eddy Simulations of Non-Premixed Turbulent Combustion. In *28:th Int. Symp. on Comb.*

Poinsot, T. and Veynante, D. (2001). *Theoretical and Numerical Combustion*. Edwards, Philadelphia.

Pope, S. B. (1990). Computations of turbulent combustion: Progress and challenges. In *23:rd Int. Symposium on Combustion*, page 591.

Sandia (2003). http://www.ca.sandia.gov/tnf/dataarch/sandchn.html. Internet.

van Kalmthout, C. M. (1986). *Stabilisation et modelisation des flammes turbulentes non premelangees. Etude theorique et simulations directes*. PhD thesis, Ecole Centrale de Paris.

Vervish, L. and Poinsot, T. (1998). Direct numerical simulation of non-premixed turbulent flames. *Annual Rev. Fluid Mech.*, **30**:655–692.

Weller, H. G., Tabor, G., Jasak, H., and Fureby, C. (1997). A tensorial approach to CFD using object oriented techniques. *Computations in Physics*, **12**:629.